JOC The Journal of Organic Chemistry

pubs.acs.org/joc Article

Structural Diversity of Perylenequinones Is Driven by Their Redox Behavior

Zeinab Y. Al Subeh, Amy L. Waldbusser, Huzefa A. Raja, Cedric J. Pearce, Kin Lok Ho, Michael J. Hall, Michael R. Probert, Nicholas H. Oberlies,* and Shabnam Hematian*

Cite This: J. Org. Chem. 2022, 87, 2697−2710 Read Online

ACCESS | Metrics & More | Article Recommendations | Supporting Information

ABSTRACT: Hypocrellins and hypomycins are two subclasses of fungal perylenequinones with unique structural, biological, and photochemical properties. With the growing interest in these naturally occurring photosensitizers, more studies were warranted to better understand the structural relationships between these two subclasses of perylenequinones. In this study, the long-postulated biosynthetic precursor (**7**) of class B fungal perylenequinones was isolated and characterized from a *Shiraia*-like sp. (strain MSX60519). Furthermore, the electrochemical and chemical redox behaviors of hypocrellins and hypomycins were investigated under aerobic and anaerobic conditions. These studies served to define the structural relationship within hypocrellins (**1**−**3**), which was further supported by X-ray crystallography, and between hypocrellins and hypomycins (**4**−**6**). Chemical reductions of hypocrellins under anaerobic conditions identified the origin of hypomycin A (**4**), hypomycin C (**5**), and hypomycin E (**6**), which in turn served to confirm **4** and revise the absolute configurations of **5** and **6**. Hypocrellins were shown to undergo reversible reduction and reoxidation under aerobic conditions, while in an anaerobic environment and longer time scale, the fully reduced form can, to some extent, undergo an intramolecular ring closing metathesis. This may impart a means of reductive pathway for self-protection against these phototoxins and explain the chemical diversity observed in the fungal metabolites.

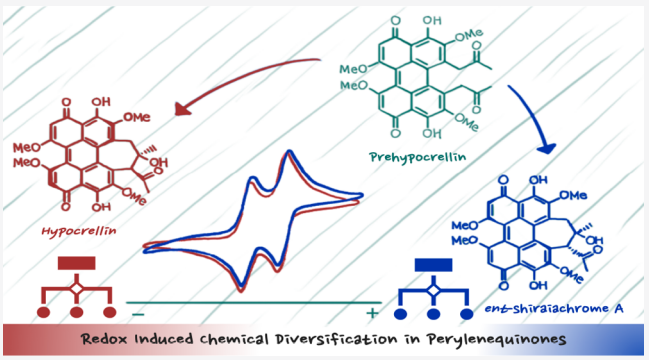

INTRODUCTION

Hypocrellins, a subclass of perylenequinones, have gained interest in photodynamic therapy as naturally occurring photosensitizers,[1−4] with hypocrellin, its enantiomer (hypocrellin A), hypocrellin B, and shiraiachrome A as the main members of this class of fungal metabolites.[5] We recently reported the isolation of *ent*-shiraiachrome A (**1**), the shiraiachrome A enantiomer, as a major constituent in the extract of *Shiraia*-like sp. (strain MSX60519).[6,7] In addition, hypocrellin (**2**), hypocrellin B (**3**), and three hypomycins [hypomycin A (**4**), C (**5**), and E (**6**)] were isolated from the same fungus (Chart 1).[6,7] Hypomycins are structurally similar to hypocrellins but with an additional six-membered ring and a less extended conjugated π-system, which is due to the absence of the Δ1(2) double bond (Chart 1).[8,9] The biosynthetic gene clusters responsible for the biosynthesis of some fungal perylenequinones, i.e., cercosporin, hypocrellin A, and elsinochrome C, have been identified.[10−13] However, the key biosynthetic steps involved in the generation of hypocrellins, such as the formation of the seven-membered ring, remain unresolved. Moreover, studies on the biosynthesis of hypomycins have never been reported.

In previous work, we also showed that exposure to light was important for the biosynthesis of both hypocrellins and hypomycins, with approximately 70- and 20-fold improvements in the production of hypocrellins (**1**−**2**) and hypomycins (**4**−**6**), respectively, when the fungi were grown under either continuous exposure to white LED light or under 12/12 h light/dark cycles as compared to complete darkness.[6] Additionally, these two structural classes displayed potent cytotoxic activity against human skin melanoma cancer cells (SK-MEL-28) when exposed to light,[6] and they are known to exhibit a broad-range of toxicities against bacteria and fungi.[3,4,14,15] These interesting properties and findings have raised many questions, especially with respect to the biosynthesis of these perylenequinones. For instance, how does exposure to light not negatively impact the growth of the fungus? In other words, how do hypocrellin-producing fungi

Received: October 28, 2021
Published: January 25, 2022

https://doi.org/10.1021/acs.joc.1c02639
J. Org. Chem. 2022, 87, 2697−2710

Chart 1. Structures of the Hypocrellins (1−3) and Hypomycins (4−6) Discussed in This Study[a]

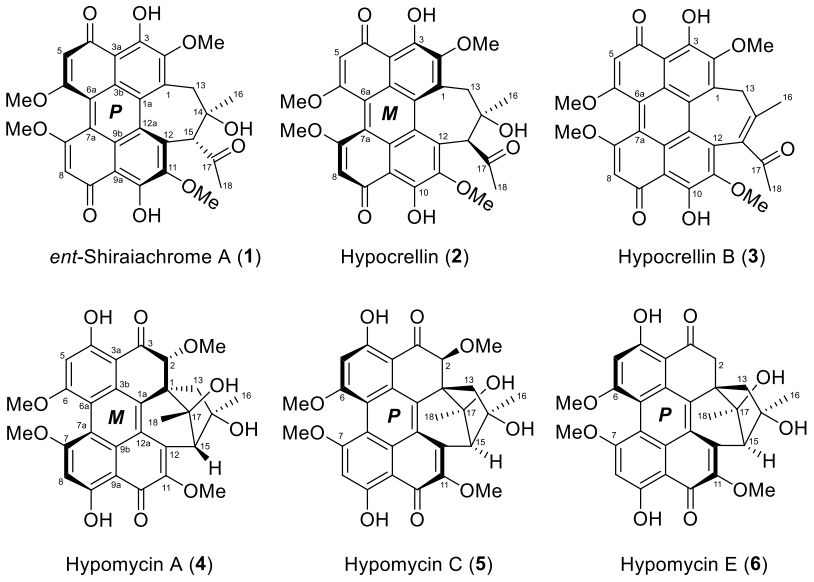

[a]*Note:* The absolute configurations of **5** and **6** are revised relative to what was proposed originally.[6,7]

protect themselves against their own phototoxins? In addition, is it possible that hypocrellins serve as the biosynthetic precursors for hypomycins, and if so, what are the requirements for converting hypocrellins into hypomycins?

The mechanism used by hypocrellin-producing fungi to avoid self-toxicity has not been reported; however, evidence from fungi that produce the structurally related compound, cercosporin, suggested the ability of fungi to reduce and detoxify this photosensitizer (Figure S1).[16−18] The reduced form of cercosporin has been shown to be a species with little photosensitizing capacity, resulting in diminished toxicity as compared to the parent cercosporin.[19−21] Given the structural similarities between hypocrellins and cercosporin (Figure S1), it was conceivable that hypocrellin-producing fungi adapt similar mechanisms to protect themselves against these native photosensitizers.

A goal of this study was to better understand the biosynthetic relationships between hypocrellins and hypomycins via examining the origins of the structural diversity for these two subclasses of perylenequinones. To do so, we investigated their redox activities to probe the potential ability of hypocrellin-producing fungi to reduce and, hence, detoxify these perylenequinones. Here, we present the isolation and characterization of the long-proposed naturally occurring biosynthetic precursor of hypocrellins. Furthermore, our electrochemical measurements revealed that the reduction of hypocrellins can take place at milder reducing conditions relative to hypomycins. We also report different results for the chemical reduction of hypocrellins using sodium dithionite ($Na_2S_2O_4$) under either aerobic or anaerobic conditions. Surprisingly, anaerobic reduction of hypocrellins led to the formation of hypomycins, suggesting both a means for hypocrellins-producing fungi to modulate the toxicity of these compounds and a source for the structural diversity of hypomycins.

■ RESULTS AND DISCUSSION

The questions of this study were probed via three interconnected phases. Initially, a scaled-up culture of fungal strain MSX60519 led to the isolation and elucidation of the suggested biosynthetic precursor of hypocrellins. Next, physical techniques, including cyclic voltammetry and UV−vis spectroelectrochemistry, were used to examine the electrochemical reversibility of the two one-electron reduction events of hypocrellins and the absorption profiles of the semiquinone (i.e., one-electron reduced) and hydroquinone (i.e., two-electron reduced) forms of *ent*-shiraiachrome A (**1**). In addition, chemical reduction of hypocrellins under aerobic conditions led to a suite of demethylated derivatives. Strikingly, under anaerobic conditions, hypocrellins were converted into hypomycins, and a series of demethoxylated derivatives were also observed. This anaerobic reduction study, along with the ^{1}H NMR characterizations, comparisons of the intramolecular hydrogen bonds, and ECD calculations, led to revisions in the structures of hypomycin C (**5**) and E (**6**). Finally, this study also provided the first X-ray crystal structures of both *ent*-shiraiachrome A (**1**) and hypocrellin B (**3**).

Identification of the Potential Precursor of Hypocrellins. To secure larger quantities of hypocrellins, particularly *ent*-shiraiachrome A (**1**), cultures of strain MSX60519 were grown on rice medium with exposure to white LED light, replicating conditions reported earlier.[6] The resulting extract (1.7 g) yielded 580 mg of **1**, 23 mg of **2**, and 0.5−5.0 mg of **3**−**6**. In addition, a benefit of scaling the biosynthesis of fungal metabolites is the identification of other minor constituents,[22,23] and in this case a new hypocrellin-like compound (**7**, 1.5 mg) was identified through high resolution electrospray ionization mass spectrometry (HRESIMS) and UV−vis absorption spectroscopy (Figures S2 and S3). The molecular formula of **7**, as deduced from the HRESIMS data (measured *m*/*z* 547.1583 $[M + H]^+$ vs calculated 547.1604), was similar to that reported for **1** and **2** ($C_{30}H_{26}O_{10}$). However, the ^{1}H- and $^{13}C\{^1H\}$-NMR data revealed only 13 proton and 15 carbon signals, suggesting a symmetrical structure (Table S1 and Figure S4). Examination of the 1D and 2D NMR spectra confirmed the characteristic conjugated pentacyclic core of perylenequinones in **7** (Figures S4−S8). However, the unsymmetrical seven-membered carbocyclic ring was missing

https://doi.org/10.1021/acs.joc.1c02639
J. Org. Chem. 2022, 87, 2697−2710

in 7, being replaced by 2-propanone side chains attached at C-1 and C-12 of the pentacyclic core (Chart 2). This compound was ascribed the trivial name prehypocrellin (7).

Chart 2. Structure of Compound 7 (A) as Compared to the Synthetic Precursor Used in the Total Synthesis of Hypocrellin A (B) as Reported by O'Brien *et al.*[24]

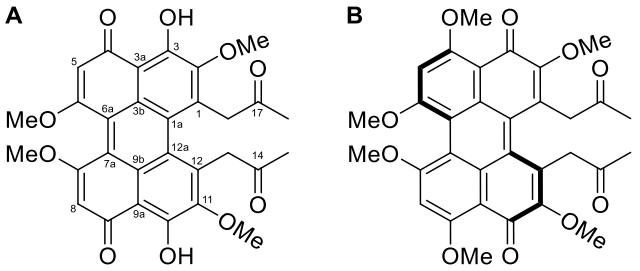

We propose that compound 7 represents a common intermediate in the biosynthetic pathway of compounds in the hypocrellin family. The structural similarity between 7 and the synthetic precursor used in the total synthesis of hypocrellin A, as described by O'Brien *et al.* (Chart 2),[24] supports this conclusion. In fact, the structure of 7 was suggested as a plausible biosynthetic intermediate for a variety of fungal perylenequinones,[24−27] although it has never been reported from nature. In this context, compound 7 may follow a variety of biotransformation paths to yield the structural diversity seen with perylenequinones, and the isolation of this biosynthetic intermediate further supports what had been hypothesized in the literature, that a common biosynthetic intermediate is responsible for the pentacyclic core and the common substituents for compounds in class B perylenequinones, including cercosporin-like compounds, elsinochromes, and hypocrellins.[27] For instance, reduction of the ketone moieties at C-14 and C-17 could result in compounds like calphostins, phleichromes, and cercosporin (Scheme 1). Alternatively, oxidative enol coupling could generate products like the elsinochromes, while diastereoselective aldol cyclization may generate hypocrellin derivatives (Scheme 1). Interestingly, compound 7 displayed no observable peaks in its Electronic Circular Dichroism (ECD) spectrum (Figure S20). This could be attributed to the presence of a racemic mixture of two possible atropisomers; a similar observation was reported previously for hypocrellin B (3) (Figure S20).[6,28,29] In fact, a number of natural and synthetic perylenequinones have been shown to have relatively low barriers for interconversion between the two possible atropisomers. In the case of the hypocrellins (**1**−**3**), the additional seven-membered ring attached to the pentacyclic core lowers their barrier of atropisomerization, such that it can be observed at room temperature.[6] The isolation of only a relatively small amount of 7 (1.5 mg), even from a scaled-up fungal culture, could be attributed to the high reactivity of this biosynthetic intermediate and its facile conversion into other perylenequinone derivatives.

Electrochemical Study of Hypocrellins and Hypomycins. To compare the redox behaviors of both hypocrellins (**1**−**3**) and hypomycins (**4**−**6**), cyclic voltammetry measurements were conducted in acetonitrile (CH_3CN) containing 100 mM of *tetra-n*-butylammonium hexafluorophosphate $[(n\mathrm{Bu})_4\mathrm{N}][\mathrm{PF}_6]$ as the supporting electrolyte under rigorous air-free conditions (Figure 1). All potential values are reported against the silver/silver chloride (Ag/AgCl) reference electrode. The voltammograms of the hypocrellin molecules (i.e., **1**−**3**) in aprotic media showed two successive quasi-reversible one-electron reduction processes (Figure 1).

The first reduction event represents the formation of the semiquinone radical anion form ($SQ^{\bullet-}$) of hypocrellins (**1**−**3**) with half-wave potentials ($E_{1/2}$) ranging from −0.46 V to −0.51 V (Figure 1 and Table S2). The second reduction event gave rise to hypocrellins in the dianion (Q^{2-}) state with $E_{1/2}$ ranging from −0.71 V to −0.76 V (Figure 1 and Table S2). Interestingly, the presence of the additional π-bond between

Scheme 1. Compound 7 as a Common Precursor for Class B Perylenequinones

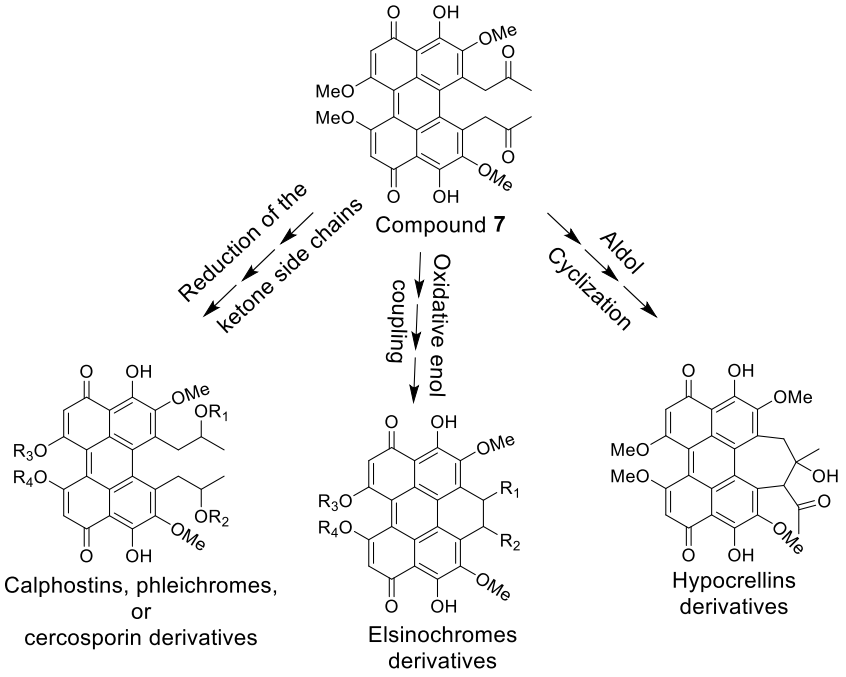

https://doi.org/10.1021/acs.joc.1c02639
J. Org. Chem. 2022, 87, 2697−2710

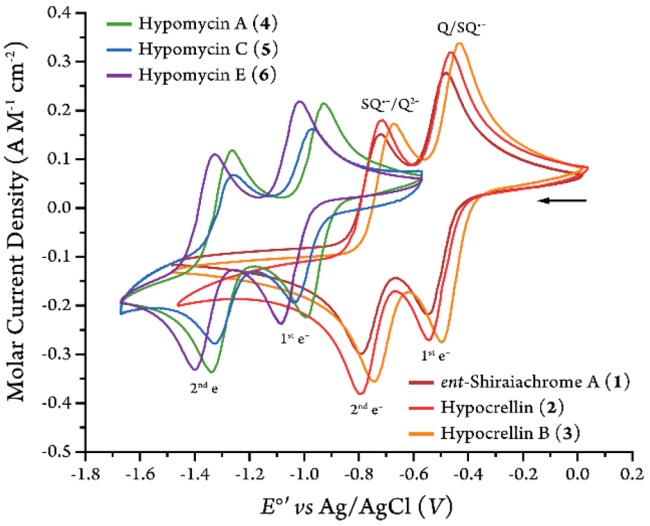

Figure 1. Normalized cyclic voltammograms of hypocrellins (**1**−**3**) and hypomycins (**4**−**6**) in CH_3CN with 100 mM of $[(n\text{Bu}_4)\text{N}][PF_6]$ as the supporting electrolyte. **Q**: quinone form. **SQ**$^{\bullet-}$: semiquinone radical anion form. **Q**$^{2-}$: hydroquinone dianion form.

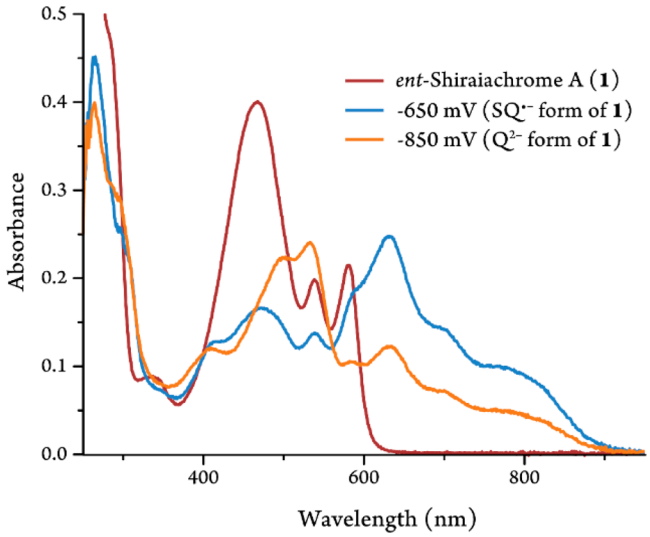

Figure 2. UV−vis spectroelectrochemical spectra of the first (semiquinone radical anion form, SQ$^{\bullet-}$) and second (hydroquinone form, Q^{2-}) reductions of *ent*-shiraiachrome A (**1**) (248 μM) in CH_3CN with 0.1 M $[(n\text{Bu})_4\text{N}][PF_6]$ as the supporting electrolyte.

C-14 and C-15 in hypocrellin B (**3**), which is in conjugation with the sp^2-hybridized perylenequinone core, led to easier first- and second-electron reduction processes, as **3** has the least negative values of the $E_{1/2}$, followed by **1** and **2**. Hypomycins (i.e., **4**−**6**) also showed two one-electron quasi-reversible reduction events, and as expected with the less extended conjugated π-system in the pentacyclic core, their $E_{1/2}$ values were more negative, ranging from −0.96 V to −1.05 V and −1.29 V to −1.36 V for the first and second reduction events, respectively (Figure 1 and Table S2). Additionally, the absence of the inductive electron-withdrawing effect of a methoxy group at C-2 in hypomycin E (**6**) resulted in more difficult first- and second-electron reduction processes, as **6** had the most negative $E_{1/2}$ values, followed by **4** and **5**. The peak-to-peak separations (i.e., $\Delta E_{1/2}$ ranging from 60 to 80 mV) and anodic/cathodic peak current ratios (i.e., i_{pa}/i_{pc} = 0.90−1.12) for compounds **1**−**6** are presented in Table S3. In aqueous acetate buffer at pH = 5, the reduction involved a single step two-electron two-proton process (e.g., for **3** $E_{1/2}$ = −0.417 V vs Ag/AgCl and $\Delta E_{1/2}$ = 88 mV; Figure S9).

Further characterization for the semiquinone radical anion and hydroquinone dianion forms of *ent*-shiraiachrome A (**1**) was performed using UV−vis spectroelectrochemistry. Initially, the UV−vis spectrum was collected for **1** in its starting quinone form, showing maximum absorption in the blue region (λ_{max} = 430 nm) along with two weaker electronic absorptions at 540 and 580 nm (Figure 2). At −650 mV, where the semiquinone radical anion form of **1** would be the most dominant species, the UV−vis spectrum showed a more extended absorption profile in the visible and near-IR (vis−NIR) regions with the maxima in the red region (λ_{max} = 640 nm). The dianion form of **1** was dominant at −850 mV, which showed two strong electronic absorptions at 500 and 530 nm. The reduced forms of *ent*-shiraiachrome A (**1**) absorb blue light with lower intensities as compared to the starting quinone form (Figure 2), and their photochemical behaviors (i.e., the nature of the excited electronic states and relaxation mechanisms) are remarkably different. Accordingly, unlike the photoactivated (i.e., excited electronic state) *ent*-shiraiachrome A (**1**), which reacts with dioxygen ($^3O_2$) through direct energy transfer to generate singlet dioxygen ($^1O_2$),[6] the reduced form of **1** is expected to react with dioxygen in its ground electronic state through an electron transfer process, in the absence of proton transfer, producing superoxide ($O_2^{\bullet-}$) or peroxide (O_2^{2-}) species. Therefore, a significantly lower phototoxicity of the reduced form of **1**, as compared to the starting quinone form, is expected. This further supports our supposition that fungi convert the photoactive forms of these metabolites into the reduced (i.e., nontoxic) forms as a self-protection mechanism. Similar observations were reported for the reduced derivatives of cercosporin,[17,21] suggesting that this could be a universal trait for these perylenequinones.

Chemical Reduction of Hypocrellins and Hypomycins under Aerobic Conditions. Since the cyclic voltammograms of hypocrellins (**1**−**3**) confirmed the electrochemical reversibility of their reduction processes, chemical reductions of these three compounds were performed using sodium dithionite ($Na_2S_2O_4$). As a start, these reactions were conducted at a small scale (∼1 mg of each compound) under ambient conditions to maintain an adequate supply of O_2. Treating the deep red solutions of **1**−**3** individually in CH_3CN with excess amounts of $Na_2S_2O_4$ aqueous solution resulted in an immediate color change from deep red to yellow (Figure S10A and B), representing the formation of the reduced hydroquinone forms of **1**−**3**. Subsequently, the reversible reaction of the hydroquinone forms with O_2 was observed *via* the development of the red color as air diffused into the solutions (Figure S10C). This indicated that compounds **1**−**3** were spontaneously reduced to the yellow hydroquinone forms in the presence of the appropriate reducing agent and were readily oxidized back to the red quinone forms through reacting with O_2. The UPLC-HRESIMS data for the reaction mixtures of **1**−**3** confirmed the recovery of the original compounds in the quinone form, rather than the hydroquinone form (Figures S11−S13). In addition, a series of other side products were produced during these redox interconversions. The molecular formulas of these products, as deduced by HRESIMS, indicated the loss of one and/or two of the methyl

https://doi.org/10.1021/acs.joc.1c02639
J. Org. Chem. 2022, 87, 2697−2710

Scheme 2. Generation of 8−10 via Reduction of *ent*-Shiraiachrome A (1) under Aerobic Conditions

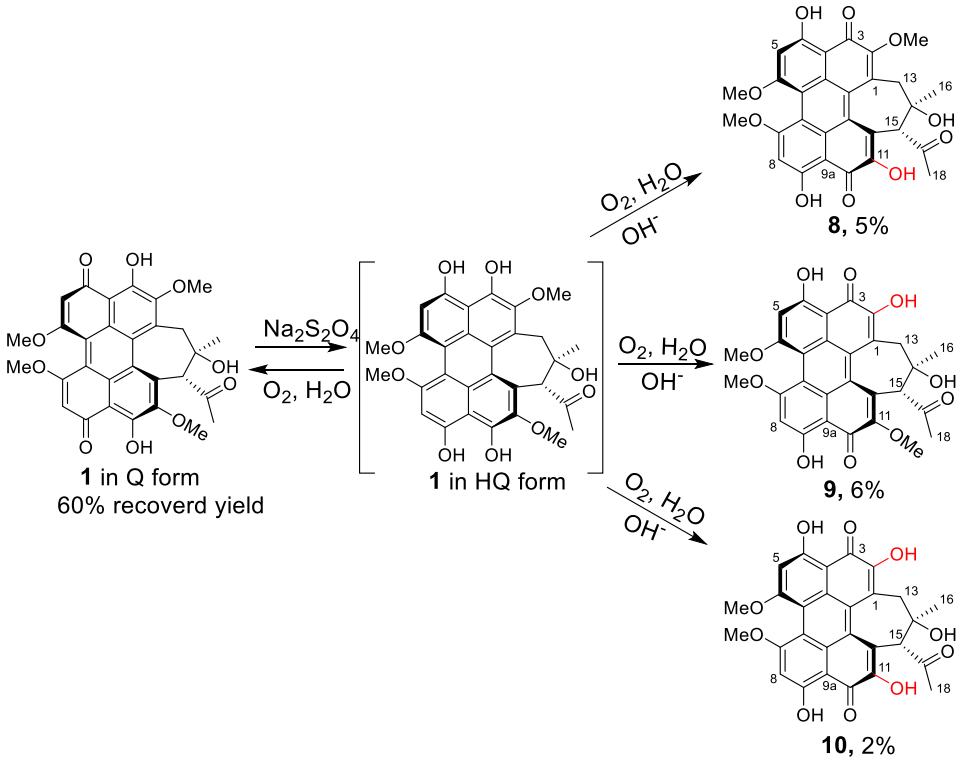

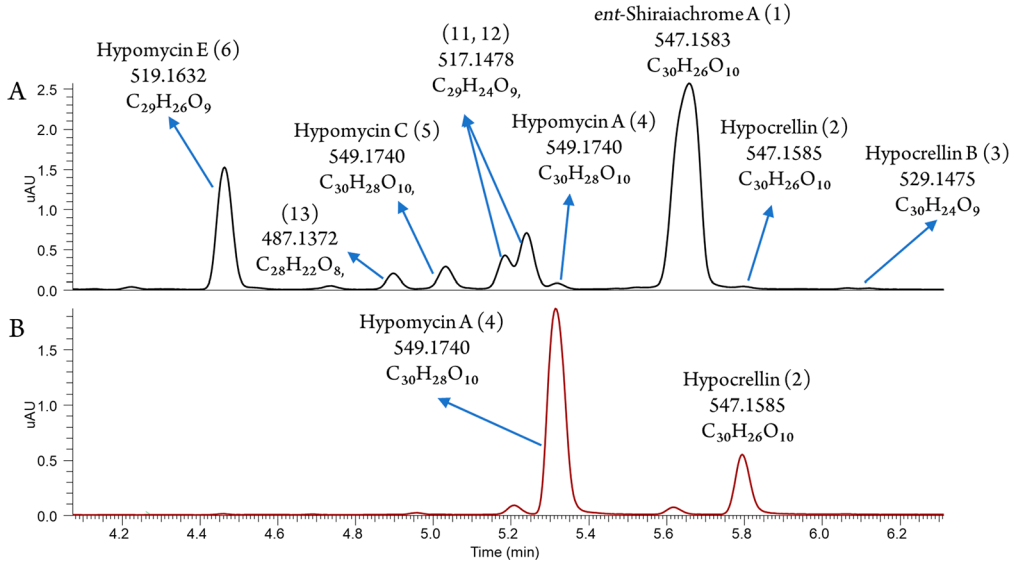

Figure 3. UPLC-HRESIMS chromatogram of anaerobic reduction reaction of (A) *ent*-shiraiachrome A (**1**) and (B) hypocrellin (**2**). HRESIMS data are reported as $[M + H]^+$.

groups in the structures of **1**−**3** (Figures S11−S13). To further characterize these derivatives, scaled-up reduction reactions of 10 mg of *ent*-shiraiachrome A (**1**) with $Na_2S_2O_4$ were conducted in four replicates (total of 40 mg). Subsequently, the reaction mixtures were subjected to UPLC-HRESIMS, where the four reactions showed the same side products observed in the small-scale reduction reaction of **1** (Figure S14). The reaction mixtures were then combined and subjected to preparative HPLC to obtain compounds **8**−**10**, in addition to the recovery of **1** in the quinone form (Scheme 2). The structures of **8**−**10** were characterized by analyzing HRESIMS data and 1D and 2D NMR spectra (Table S4 and Figures S15−S18). Accordingly, the methoxy groups attached to C-11 in **8**, C-2 in **9**, and both C-11 and C-2 in **10** were replaced with hydroxy moieties. Compounds **8**, **9**, and **10** were generated in approximately a 3:3:1 ratio, respectively (Scheme 2). The replacement of one or both methoxy groups at these positions (i.e., C-2 and C-11) by hydroxy groups is in excellent agreement with previous reports on simpler quinone systems that show that these positions were susceptible to nucleophilic substitution.[30] Note that during this process the location of the oxidized half of the perylenequinone structures are shifted from the left side in **1** to the right side of the molecule in **8**−**10**, so that the methoxy groups adjacent to the carbonyl sites

https://doi.org/10.1021/acs.joc.1c02639
J. Org. Chem. 2022, 87, 2697−2710

Scheme 3. Derivatives Obtained by Chemical Reduction of *ent*-Shiraiachrome A (1) with $Na_2S_2O_4$ under Anaerobic Condition

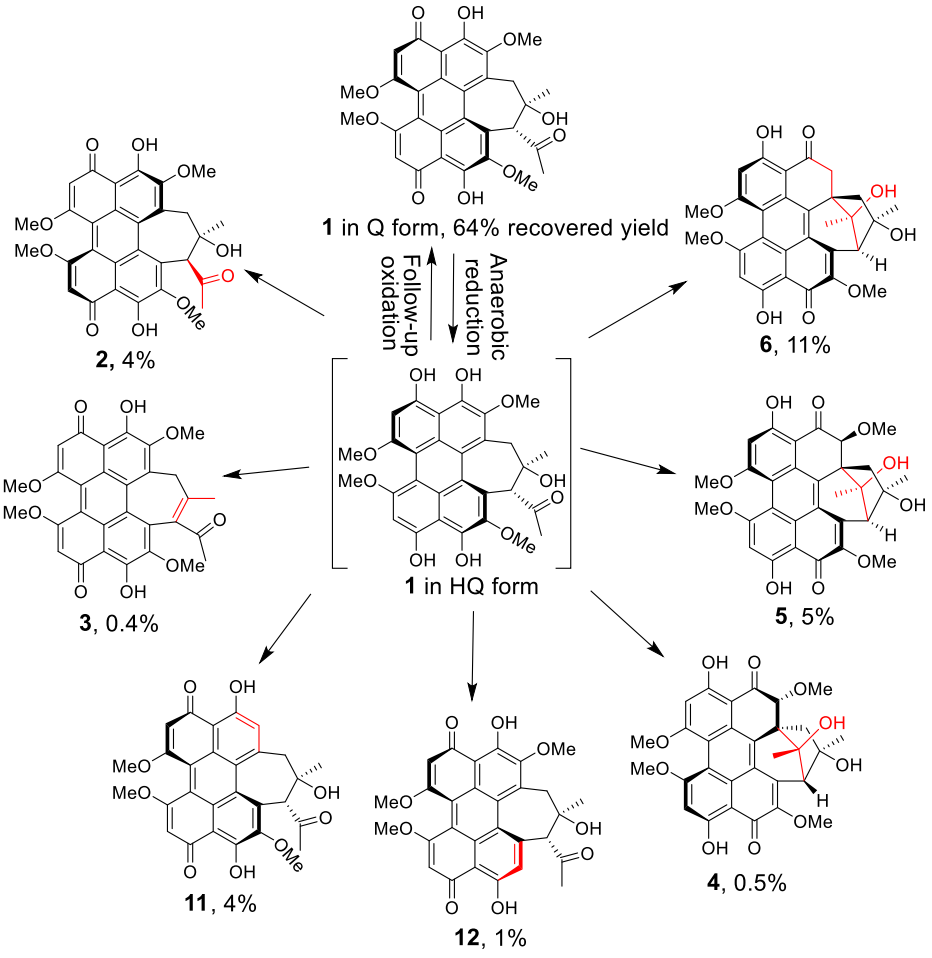

are replaced by hydroxy moieties. This observation is also consistent with the fact that, during the aerobic reduction of these hypocrellins with a limited proton source (i.e., in the form of water), dioxygen molecules were continuously reduced and converted to hydroxide ions, thus acting as effective nucleophiles. The tautomeric structures of **8**−**11** were established by examining their HMBC spectra (Figure S18). Compounds **8**−**10** exhibited the characteristic electronic absorption profile of perylenequinones (Figure S19) and maintained the same axial chirality of *ent*-shiraiachrome A (**1**), as noted by their ECD spectra (Figure S21).

Similar experiments with the hypomycins (i.e., **4**−**6**) resulted in no detectable substitution of the methoxy groups, one of which is attached to an sp^3 carbon in hypomycins (i.e., C-2). Here, aerobic reduction with $Na_2S_2O_4$ led to the full recovery of the original hypomycins in their quinone forms (Figures S22−S24). Moreover, as expected, no apparent color change was observed during the reduction process (Figure S25). Indeed, the electronic absorption profiles of hypomycins in the visible region are significantly different than hypocrellins, in that the former are yellow to orange-colored (Figure S26), as opposed to the deep red-color noted with hypocrellins (Figure S10).

Chemical Reduction of Hypocrellins under Anaerobic Conditions. As the aerobic chemical reduction of hypocrellins (**1**−**3**) resulted in a series of demethylated analogues as minor products, we investigated this reaction under anaerobic conditions. *ent*-Shiraiachrome A (**1**, 10 mg) was treated with excess $Na_2S_2O_4$ under argon in triplicate (total of 30 mg of **1**). UPLC-HRESIMS data of the reaction mixtures confirmed the recovery of **1** in the quinone form as a major product (64%) (Figure S27). Surprisingly, eight other derivatives were also detected, and this was observed consistently across triplicate reactions (Figures 3A and S27). Based on matching the UPLC retention time and HRESIMS data, these products were identified as hypocrellin (**2**), hypocrellin B (**3**), hypomycin A (**4**), hypomycin C (**5**), and hypomycin E (**6**) (Figure S28). Three new products were also identified (i.e., **11**−**13**) with molecular formulas of $C_{29}H_{24}O_9$ for both **11** and **12** and $C_{28}H_{22}O_8$ for **13** as deduced by HRESIMS data (Figure 3A). Accordingly, these compounds were missing either one (as in **11** and **12**) or two methoxy groups (as in **13**) relative to the starting compound (**1**). The generation of these natural (**2**−**6**) and un-natural (**11**−**13**) analogues through the anaerobic reduction of **1** suggests that the structural diversity of hypocrellins and hypomycins derives from their redox activities, which in some cases are followed by intramolecular or intermolecular nucleophilic reactions, *vide infra*.

To facilitate the isolation of the products, the anaerobic reaction was repeated using 50 mg of **1** followed by preparative HPLC to obtain **1**−**6** and **11**−**12** (Scheme 3). The structures were confirmed by ^{1}H NMR and ECD spectra as compared to those reported previously (Figure S29).[6,7] Aside from the recovered *ent*-shiraiachrome A (**1**), the highest yield was for hypomycin E (**6**; ∼11%) followed by hypomycin C (**5**; ∼5%). Hypomycin A (**4**) was isolated in low yield (∼0.5%) from the

https://doi.org/10.1021/acs.joc.1c02639
J. Org. Chem. 2022, 87, 2697−2710

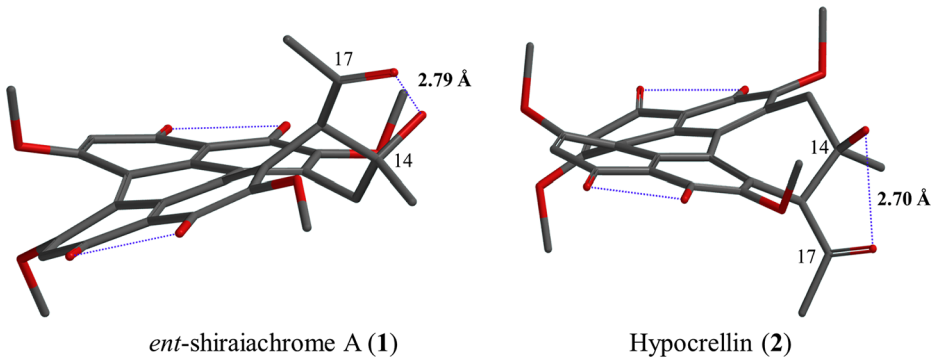

Figure 4. Intramolecular hydrogen-bonding between the C-14 hydroxy and the C-17 carbonyl groups in the 3D structures of *ent*-shiraiachrome A (**1**) and hypocrellin (**2**). The donor−acceptor distance of 2.70 Å in **2** and 2.79 Å in **1** indicates stronger hydrogen-bonding in hypocrellin (**2**). The 3D molecular structures and donor−acceptor distances of the intramolecular hydrogen bonding interactions were obtained through Spartan'10 (version 1.1.0) similarity analysis.

Scheme 4. Keto-Enol Tautomerism of *ent*-Shiraiachrome A (1) at C-17 Carbonyl Intermediates the Conversion Process of 1 into 2

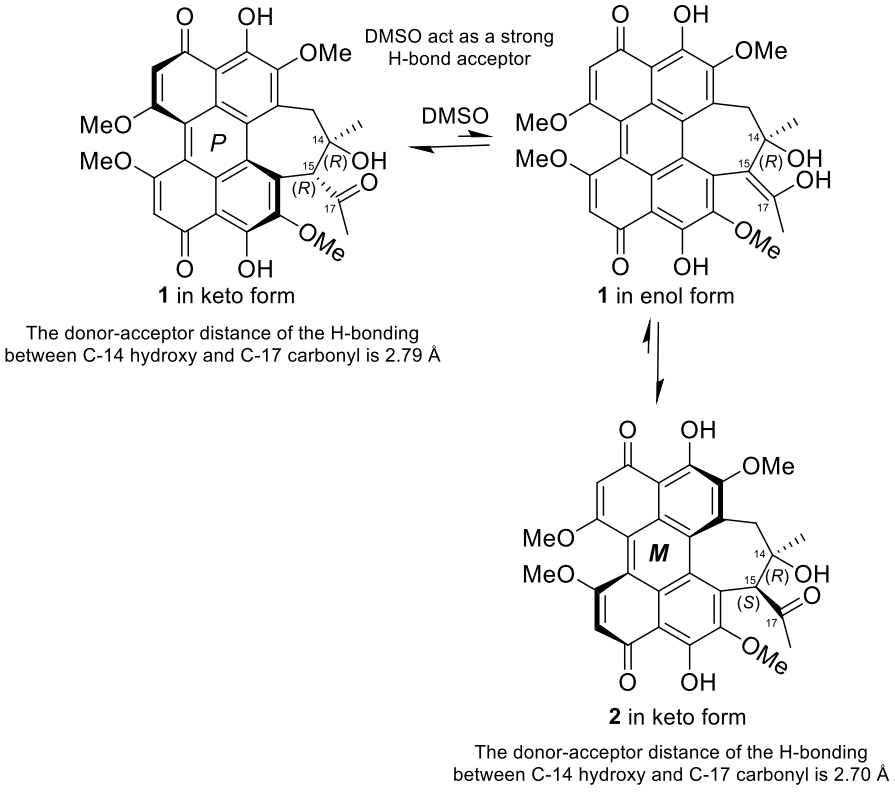

anaerobic reduction of **1** (Figure 3A). This was somewhat surprising, as hypomycin A (**4**) showed the highest abundance in the extract of strain MSX60519 as compared to **5** or **6**.[6] This led us to propose that hypomycin A (**4**) is a derivative of hypocrellin (**2**) rather than *ent*-shiraiachrome A (**1**), particularly since the axial chirality of **4** matches that of **2** (i.e., *M*; Chart 1) rather than that of **1** (i.e., *P*; Chart 1). In this context, we proposed that the reduction of **1** led to the generation of **2**, which in turn underwent anaerobic reduction to provide hypomycin A (**4**).

To test this hypothesis, 4.6 mg of pure hypocrellin (**2**) were reduced using $Na_2S_2O_4$ under anaerobic conditions, and the UPLC-HRESIMS data of the reaction mixture showed the production of hypomycin A (**4**) in a relatively high yield (~65%), in addition to the recovery of **2** in the quinone form (~11%) (Figures 3B and S30). Interestingly, the yield of this intramolecular cyclization under anaerobic conditions to produce hypomycin A (**4**) from hypocrellin (**2**) was markedly higher as compared to the relatively low yield of hypomycin C (**5**) and E (**6**) from the anaerobic reduction of *ent*-shiraiachrome A (**1**) (i.e., 5% and 11%, respectively). This could be attributed to the stronger intramolecular hydrogen bonding present between HO-14 and the C-17 carbonyl in **2**, as evidenced by the donor−acceptor distance of 2.70 Å compared to 2.79 Å in **1** (Figure 4). This would increase the electrophilicity, and hence the reactivity, of the C-17 carbonyl in **2** to produce relatively larger amounts of **4**. These data correlated well with our previous findings, where the isolated amount of hypomycin A (**4**) was significantly higher than those of hypomycin C (**5**) and E (**6**) from fungal strain MSX60519.[6]

https://doi.org/10.1021/acs.joc.1c02639
J. Org. Chem. 2022, 87, 2697−2710

Therefore, we postulate that the hypomycins (**4**–**6**) could derive from the hypocrellins, meaning that their production requires the reduction of the appropriate hypocrellins under anaerobic conditions. Indirectly, this indicates the ability of fungi to reduce various hypocrellins under oxygen-free conditions to generate a variety of hypomycins;[31] a finding that is consistent with reports of oxidoreductases in diverse groups of fungi.[32−34] More recently, the sporocarp environment in some fungi has been reported to be anoxic, and this includes a thick outer covering to protect the oxygen-sensitive nitrogenase enzyme, indicating the ability of fungi to create anaerobic environments despite the fact that they live in aerobic habitats.[35] Other evidence from the literature that supports this conclusion is the recent discovery of hypomycin A enantiomer, (*P*)-hypomycin A, from the stromata extract of *Hypocrella bambusae*, where hypocrellin A (i.e., the hypocrellin enantiomer) was the major constituent in the extract.[15] Accordingly, to satisfy the absolute configurations among related molecules, hypomycin A (**4**) with an absolute configuration of *M*(*R*), 1*S*, 2*R*, 14*R*, 15*S*, 17*R* would derive from hypocrellin (**2**) with an absolute configuration of *M*(*R*), 14*R*, 15*S*, while (*P*)-hypomycin A (enantiomer of **4**) with an absolute configuration *P*(*S*), 1*R*, 2*S*, 14*S*, 15*R*, 17*S* would derive from hypocrellin A (enantiomer of **2**) with an absolute configuration of *P*(*S*), 14*S*, 15*R*.[6,15]

The conversion of *ent*-shiraiachrome A (**1**) to hypocrellin (**2**) was an interesting observation, as this required flipping the axial chirality from *P*(*S*) in **1** to *M*(*R*) in **2**, along with changing the configuration at C-15 from 15*R* in **1** to 15*S* in **2** (Chart 1). From our ^{1}H NMR measurements, we believe that the intramolecular hydrogen bonding between the C-17 carbonyl and C-14 hydroxy maintains the structures of **1** and **2** in the keto form at C-17 (Figure 4) in solution, and the presence of this intramolecular hydrogen bonding interaction in the solid state was also previously confirmed in the X-ray crystal structure of **2**.[36] Accordingly, the 15*R* configuration goes with the *P*(*S*) chirality, as seen in **1**, while the 15*S* configuration goes with the *M*(*R*) chirality, as seen in **2**.

In theory, conversion of **1** into **2** can be achieved through keto−enol tautomerism at the C-17 carbonyl (Scheme 4). The enol form of **1** could be favored if the hydrogen bonding between the C-17 carbonyl and C-14 hydroxy groups was disturbed, where the double bond in the enol form would be stabilized by engaging with the conjugated system of the pentacyclic core (Scheme 4). Therefore, the keto−enol tautomerism process at C-17 engenders the formation of the 15*R* stereocenter along with *P*(*S*) chirality, as in *ent*-shiraiachrome A (**1**), or the formation of the 15*S* stereocenter along with *M*(*R*) chirality, as in hypocrellin (**2**). To investigate this possibility, DMSO-d_6 was used as a hydrogen bond acceptor to dissolve a sample of *ent*-shiraiachrome A (**1**). The ^{1}H NMR spectrum of **1** in DMSO-d_6 showed broadened signals, indicating the disruption of the intramolecular hydrogen bond and the presence of a sufficiently fast equilibrium between the keto- and the enol-forms, exceeding the NMR time scale and preventing the observation of separate resonances (Figure S31). After drying the sample and recollecting the ^{1}H NMR data in $CDCl_3$, two sets of signals appeared in the spectrum. One set matched that of *ent*-shiraiachrome A (**1**), while the other set matched the ^{1}H NMR profile of hypocrellin (**2**) (Figure S32). This shows that hypocrellin (**2**) can derive from **1** simply by exposure to a solvent that is a strong hydrogen bond acceptor (e.g., DMSO), which facilitates the keto−enol tautomerism at the C-17 carbonyl, and thus, the reduction of **1** is not an essential step in the conversion of **1** into **2**. Moreover, this suggests that a similar keto−enol tautomerism at C-17 occurs between hypocrellin A (the enantiomer of **2**) and shiraiachrome A (the enantiomer of **1**), as evidenced by their concurrent isolation from various fungi.[5,15,28,29,37]

Despite the isolation of hypocrellin B (**3**) from various fungi as a naturally occurring perylenequinone, it is also known to be a dehydration product of other hypocrellins; for example, hypocrellin B (**3**) can be produced readily by simple dehydration of either hypocrellin (**2**), hypocrellin A, shiraiachrome A, or *ent*-shiraiachrome A (**1**).[6,28,29] The absence of ECD activity for **3** could result from its planar structure or, more likely, from a racemic mixture of the *M*(*R*) and *P*(*S*) enantiomers of **3**.[6,24] Following successful single crystal growth via ENaCt,[38] we report the first X-ray crystallographic structure of **3**, where a racemic mixture of the *M*(*R*) and *P*(*S*) enantiomers was observed in the solid state (Figures 5 and S33−S34). Accordingly, compound **3** exhibits a

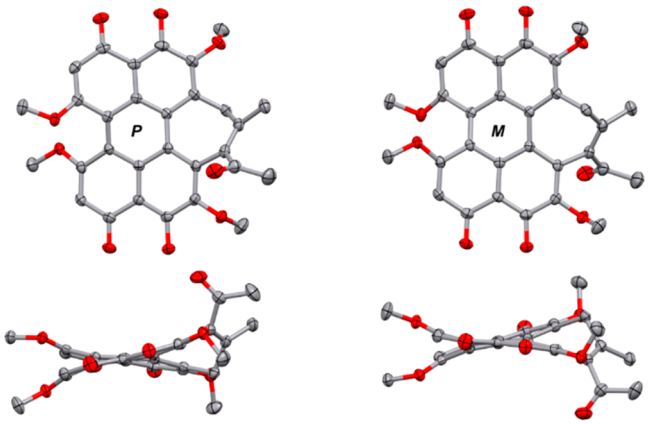

Figure 5. Two atropisomers of hypocrellin B (**3**) present in the solid state.

low barrier of atropisomerization, which can be observed at room temperature. The fact that hypocrellin B (**3**) exists as a racemic mixture of the two possible atropisomers further supports our theory that the intramolecular hydrogen bond interaction exhibits a chiral induction effect and is a major factor in determining the favored axial chirality of *ent*-shiraiachrome A (**1**) and hypocrellin (**2**), since losing that intramolecular force, as in **3**, leads to a racemic mixture of the two atropisomers.

The conversion of hypocrellins (**1** or **2**) into hypomycins (**4**–**6**) requires the reduction of hypocrellins under oxygen-free conditions, since the production of hypomycins was not observed under any other conditions (i.e., exposure to DMSO, dehydration reactions, or reduction under aerobic conditions). Although the reduction reactions were conducted in oxygen-free settings, UPLC-MS data and product purifications were performed after drying the reaction mixture under an anaerobic environment but then exposing it to normal room conditions. Thus, a question that emerged was whether hypomycins formed before or after exposing the reaction mixture to dioxygen. To probe this, ^{1}H NMR data for the reaction products of **1** and **2** were collected in deuterated CH_3CN before air exposure (Figures S35 and S36). Interestingly, the main set of peaks observed in the reduction reaction of *ent*-

https://doi.org/10.1021/acs.joc.1c02639
J. Org. Chem. 2022, 87, 2697−2710

Scheme 5. Structural Relationships between the Natural (1−7) and Non-natural (8−13) Hypocrellin Derivatives

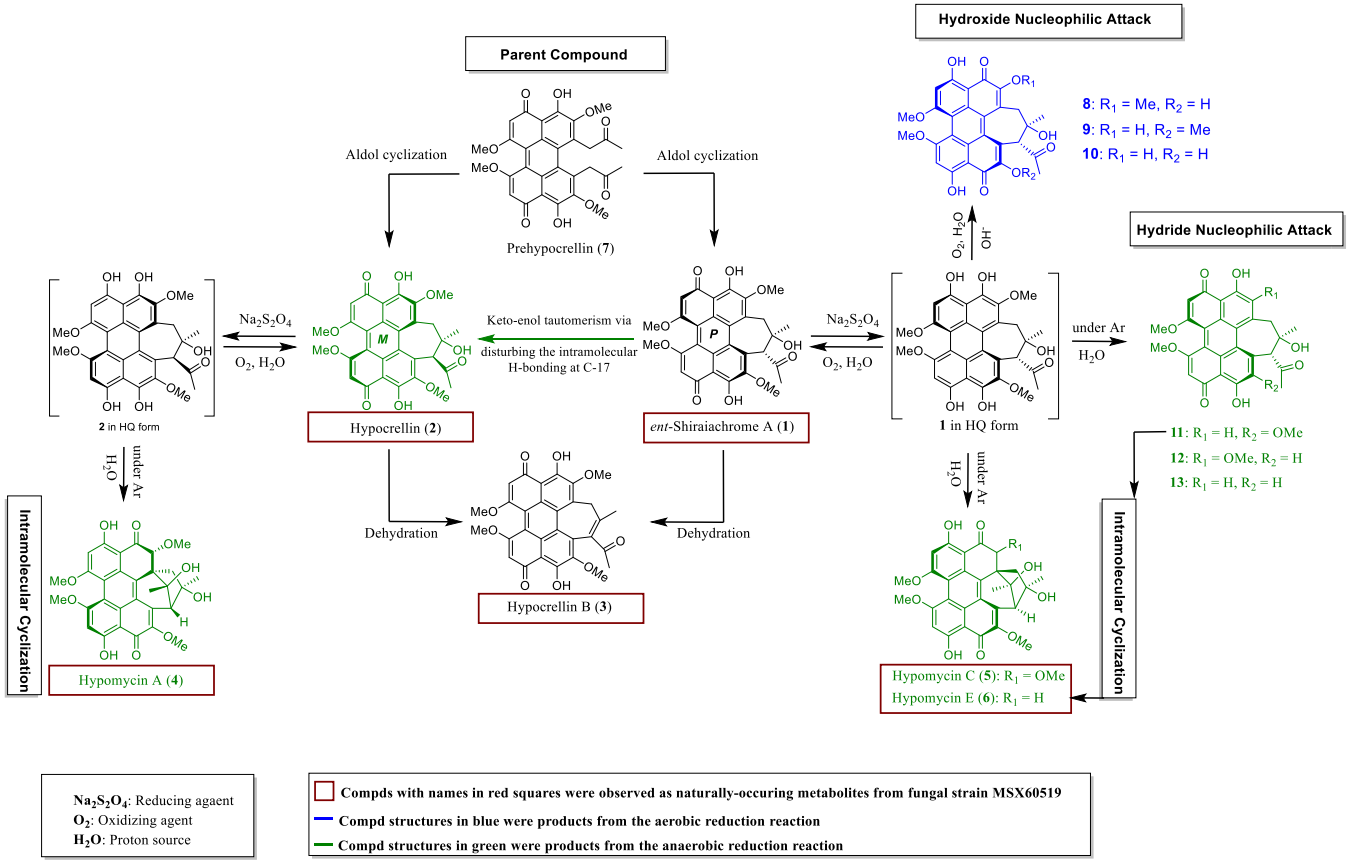

shiraiachrome A (**1**) matched those of hypomycin E (**6**) (Figure S35), while those matching hypomycin C (**5**) were at lower intensity. The anaerobic reduction reaction of hypocrellin (**2**) showed peaks that match those of hypomycin A (**4**) (Figure S36). Accordingly, we suggest that intramolecular cyclization of the hypocrellins to produce hypomycins occurs before exposure to any source of dioxygen.

In our previous work, the absolute configuration of hypomycin C (**5**) was assigned as *P*(*S*), 1*S*, 2*R*, 14*S*, 15*S*, 17*R*, and for hypomycin E (**6**) it was assigned as *P*(*S*), 1*S*, 14*S*, 15*S*, 17*R*. These conclusions were based on their ECD spectra, analysis of NOESY data, and their structural similarity to hypomycin A (**4**) (Figure S37),[6] which suggested that **5** and **4** differed in both configuration of the C-14 stereogenic center and axial chirality; compound **6** was assigned based on being a demethoxylated derivative of **5**.[6] However, the anaerobic reduction reactions of **1** and **2** revealed that hypomycin A (**4**) originates from hypocrellin (**2**), while hypomycin C (**5**) and hypomycin E (**6**) are derived from *ent*-shiraiachrome A (**1**). This new information caused us to revisit the structure elucidations of **4**−**6**. The absolute configurations of hypomycin A (**4**) and hypocrellin (**2**) were in agreement (Chart 1), where both exhibit *M*(*R*) chirality and 14*R* configuration. However, the absolute configurations of hypomycin C (**5**) and hypomycin E (**6**), which likely derive from *ent*-shiraiachrome A (**1**), and all share *P*(*S*) axial chirality, were in discord at position 14, where **1** is 14*R* but **5** and **6** were reported as 14*S* (Figure S37). Since an X-ray crystallographic structure for **1**, **5**, and **6** has yet to be reported, a suitable single crystal of **1** was prepared via ENaCt and analyzed by X-ray diffraction.[38] The resulting crystal structure allowed confirmation of the reported absolute configuration of *P*(*S*), 14*R*, 15*R* by anomalous dispersion (Flack = 0.019(5)) (Figures S38−S40).[6] Unfortunately attempts to grow single crystals of **5** and **6** suitable for X-ray diffraction analysis, using both ENaCt and classical methods, proved unsuccessful.[38] Regardless, logic would follow that compounds **5** and **6** should have the 14*R* configuration, and their NOESY spectra were reanalyzed to evaluate this (Figure S41). As suggested by the NOESY correlations of **5** and **6** (Figure S41), the order of the six-membered ring and the seven-membered ring in **5** and **6** is flipped compared to **4** (Chart 1). The orientation of these two rings and their substituents were further confirmed by examining the observed exchangeable hydroxy protons in the ^{1}H NMR spectra and the presence of intramolecular hydrogen bonding in **4**−**6** (Figure S42). The ^{1}H NMR data of hypomycin A (**4**) collected in $CDCl_3$ showed the two exchangeable hydrogens at the C-14 hydroxy (δ_H 4.81) and the C-17 hydroxy groups (δ_H 5.59),[6] which suggests that these two protons are stabilized (i.e., slower chemical exchange rate) by forming intramolecular hydrogen bonds (Figure S43). The 3D structure of **4** confirmed the presence of hydrogen bonding interactions between the C-14 and C-17 hydroxy groups (2.69 Å) (Figure S42). On the other hand, the C-17 hydroxy proton (δ_H 4.96), but not the C-14 hydroxy proton, was observed in the ^{1}H NMR data for hypomycin C (**5**) in $CDCl_3$ (Figure S44),[6] which indicated that only the C-17 hydroxy group is stabilized through hydrogen bonding with the C-2 methoxy (Figure S42). Such hydrogen bonding between C-17 hydroxy and C-2 methoxy is not possible with the previously suggested structure, as the donor−acceptor distance would be 3.86 Å. Using DMSO-d_6 as a hydrogen bond acceptor allowed for

https://doi.org/10.1021/acs.joc.1c02639
J. Org. Chem. 2022, 87, 2697−2710

observing the two exchangeable protons of the C-14 hydroxy (δ_H 4.25) and the C-17 hydroxy groups (δ_H 4.76) in **5** (Figure S45). The absence of a C-2 methoxy in **6** results in losing the hydrogen bonding with the C-17 hydroxy group (Figures S42 and S46). Therefore, neither of the exchangeable hydrogens at the C-14 and C-17 hydroxys were observed in the ^{1}H NMR of **6** in $CDCl_3$.[6] Furthermore, the calculated ECD spectrum of the newly proposed structure of **5** showed higher similarity to the experimental data as compared to the previously proposed configuration (i.e., 84% vs 72%), and only the newly proposed [*P*(*S*), 1*R*, 2*S*, 14*R*, 15*R*, 17*S*]-configuration reproduced the negative Cotton effect at 500 nm (Figure S47). Previously, the appropriate Cotton effect at 500 nm was also observed for the calculated ECD spectrum of hypomycin A (**4**) only when the correct ring order was applied.[6] Accordingly, the absolute configurations of **5** and **6** were revised to *P*(*S*), 1*R*, 2*S*, 14*R*, 15*R*, 17*S* and *P*(*S*), 1*S*, 14*R*, 15*R*, 17*S*, respectively (Chart 1).

Compounds **11** and **12** represent demethoxylated derivatives of **1**, where, in each case, one of the four methoxy groups of **1** is missing as deduced by their HRESIMS data (Figure 3A). Analysis of 1D and 2D NMR spectra of **11** confirmed the loss of the methoxy group at C-2 compared to **1** (Table S7 and Figures S48−S50). The extra aromatic proton signal at δ_H 7.25 showed HMBC correlations with C-3, C-3a, C-1a, and C-13, which supported the position of this proton at C-2 in place of the methoxy group (Table S7 and Figure S50). On the other hand, the isolated amount of **12** was small (0.49 mg) with relatively low purity (Figure S49). However, the HMBC correlations exhibited by the extra aromatic proton at δ_H 7.31 with C-9a, C-10, C-12a, and C-15 supported the loss of the methoxy group at C-11 in **12** compared to **1** (Table S7 and Figure S50). Although compound **13** was not isolated in sufficient amount to allow its full NMR-based characterization, its HRESIMS data indicated the loss of two methoxy groups compared to **1** (Scheme 3). These are suggested to be the methoxy groups at C-2 and C-11. The demethoxylation mechanism of **1** to provide **11**−**13** under anaerobic reduction conditions is similar to the demethylation observed under aerobic conditions to provide compounds **8**−**10**. However, the lack of dioxygen in the anaerobic reduction process allowed the replacement of methoxy groups at C-2 and/or C-11 in **1** by hydride ions in **11**−**13**, instead of hydroxide ions as in **8**−**10**. It has been previously reported that the heterolytic dissociation of sodium dithionite leads to formation of the hydrogen sulfoxylate ion (HSO_2^-).[39] As SO_2 is a good leaving group, HSO_2^- is known to be an effective hydride donor and can facilitate the demethoxylation of **1** to obtain **11**−**13**.[40] The axial chirality of derivatives **11**−**13** is suggested to be similar to that of the original compound (**1**), since the ECD spectrum of **11** correlated with *P*(*S*) chirality (Figure S28).

In a broad context, this study connects the structural relationships between the natural (**1**−**7**) and non-natural (**8**−**13**) hypocrellin derivatives. As illustrated (Scheme 5), prehypocrellin (**7**) is suggested as the parent biosynthetic precursor for other perylenequinones. Diastereoselective aldol cyclization of **7**, for instance, would allow the formation of *ent*-shiraiachrome A (**1**) and/or hypocrellin (**2**). Dehydration of these two compounds (**1** and **2**) leads to the production of hypocrellin B (**3**), while aerobic reduction of **1**−**3** gives rise to their demethylated derivatives (e.g., **8**−**10** from **1**) via hydroxide nucleophilic attack (Scheme 5). On the other hand, anaerobic reduction of *ent*-shiraiachrome A (**1**) and hypocrellin (**2**) leads to the formation of two classes of derivatives. These include the demethoxylated analogues of **1** (i.e., **11**−**13**), which formed via hydride nucleophilic attack, while intramolecular cyclization provides hypomycin C (**5**) and E (**6**) from the anaerobic reduction of *ent*-shiraiachrome A (**1**), and hypomycin A (**4**) from the anaerobic reduction of hypocrellin (**2**) (Scheme 5).

CONCLUSION

This study expanded our knowledge on the biosynthesis and the redox behavior of hypocrellins and hypomycins, bringing to light four new aspects to our understanding of these perylenequinones. First, the biosynthetic precursor of hypocrellins was isolated and characterized, giving tangible evidence to the ultimate precursor to not only this class of compounds but also, by analogy, to the calphostins, phleichromes, cercosporins, and elsinochromes. Second, our electrochemical measurements revealed that the hypocrellins and hypomycins undergo reversible reduction processes, with the former being more thermodynamically favored (i.e., milder redox potentials), which was further supported with our aerobic chemical reduction studies. Third, hypomycins originate from reduction of hypocrellins under anaerobic conditions, and the presence of significant amounts of hypomycins in fungal culture extracts suggests that hypocrellin-producing fungi reduce these photoactive compounds, potentially as a self-protection mechanism; this has the added benefit of generating wider chemical diversity. Finally, the reductions of hypocrellins under aerobic and anaerobic conditions helped to cement the structural relationships between these compounds, providing biogeneric insights and leading to a revision of the structures of hypomycin C (**5**) and hypomycin E (**6**) and the discovery of a series of new analogues (**8**−**12**). Moreover, X-ray crystal structures of *ent*-shiraiachrome A (**1**) and hypocrellin B (**3**) were reported for the first time.

EXPERIMENTAL SECTION

General Experimental Procedures. ECD was measured using an Olis DSM 17 ECD spectrophotometer (Olis, Inc.). UV−vis absorption spectroscopic data were collected using a Cary-60 spectrophotometer (Agilent). Electrochemical data were collected using a Bio-Logic SP-200 potentiostat. 1D and 2D NMR spectra were recorded in either $CDCl_3$, CD_3CN, or DMSO-d_6 using an Agilent 700 MHz spectrometer equipped with a cryoprobe, a JEOL ECA-500 spectrometer, or a JEOL ECS-400 spectrometer equipped with a high sensitivity JEOL Royal probe and a 24-slot autosampler. The NMR shifts were referenced to $CDCl_3$ (δ_H/δ_C 7.26/77.2), DMSO-d_6 (δ_H 2.50), or CD_3CN (δ_H 1.94). UPLC-HRESIMS data were collected via an LTQ-Orbitrap XL mass spectrometry system (Thermo Finnigan, San Jose, CA, USA) connected to a Waters Acquity UPLC system. A BEH Shield RP18 column (Waters, 1.7 μm; 50 mm × 2.1 mm) heated to 40 °C was used. The mobile phase consisted of CH_3CN-H_2O (0.1% formic acid) in a gradient system of 15:85 to 100:0 over 10 min at a flow rate of 0.3 mL/min. MS data were collected from *m*/*z* 150 to 2000 in the positive mode. All analytical and preparative HPLC experiments were carried out using a Varian Prostar HPLC system equipped with ProStar 210 pumps and a Prostar 335 photodiode array detector (PDA). HPLC data were collected and analyzed using Galaxie Chromatography Workstation software (version 1.9.3.2, Varian Inc.). For preparative HPLC, a Synergi C_{12} column (Waters, 5 μm; 250 mm × 21.2 mm) was used. Flash chromatography was carried out using a Teledyne ISCO CombiFlash Rf 200 that was equipped with both UV and evaporative light-scattering detectors and using Silica Gold columns (from Teledyne Isco).

https://doi.org/10.1021/acs.joc.1c02639
J. Org. Chem. 2022, 87, 2697−2710

All reagents and solvents were of commercially available grade, unless otherwise noted. Acetonitrile (MeCN) was used after passing through a 60-cm-long column of activated alumina (Innovative Technologies) under argon. Distilled water was further purified by a Nanopure Analytical Ultrapure Water System (Thermo Scientific) to obtain the specific resistance of 18.2 MΩ·cm at 25 °C. Deoxygenation of solvents was achieved by either repeated freeze−pump−thaw cycles or bubbling with argon for 40−60 min. Sodium dithionite (for analysis EMSURE) was purchased from Millipore Sigma.

Media and Fermentations. Fungus MSX60519 was identified as a *Shiraia*-like fungus in the family Shiraiaceae, as detailed recently,[6] and was maintained on potato dextrose agar (PDA; Difco) and transferred periodically to fresh PDA Petri plates. An agar plug from the leading edge of the PDA culture was transferred to a sterile tube with 10 mL of YESD (2% soy peptone, 2% dextrose, and 1% yeast extract). The YESD culture was grown for 7 days on an orbital shaker (100 rpm) at room temperature (~23 °C) and then used to inoculate solid fermentation media.

Twelve cultures of strain MSX60519 were grown in rice medium in 250 mL Erlenmeyer flasks as previously described.[6] To prepare rice medium, 10 g of rice were added to each flask with 20 mL of deionized water. After autoclaving, the flasks were inoculated with YESD seed cultures (described above) and incubated at room temperature for 15 days under continuous LED light exposure. These conditions were found previously to enhance the production of *ent*-shiraiachrome A (**1**) and hypocrellin (**2**) from fungus MSX60519.[6]

Extraction, Fractionation, and Isolation. Extraction of the solid cultures was performed as previously described.[6] Briefly, each culture was chopped and shaken overnight in 90 mL of 1:2 CH_3OH−$CHCl_3$. The extract was vacuum filtered, and 90 mL of $CHCl_3$ and 100 mL of DI H_2O were added to the filtrate. The mixture was stirred for 30 min and then transferred into a separatory funnel. The bottom layer was drawn off, evaporated to dryness, and then reconstituted in 100 mL of 1:1 CH_3OH−CH_3CN and 100 mL of hexanes. The biphasic solution was shaken vigorously and transferred into a separatory funnel. The CH_3OH/CH_3CN layer was drawn off and evaporated under vacuum.

The organic extracts collected from the 12 cultures were combined to provide a total of 2.2 g. These were dissolved in $CHCl_3$, adsorbed onto Celite 545, and subdivided into five fractions via normal-phase flash chromatography using a gradient solvent system of hexanes−$CHCl_3$−CH_3OH at a 35 mL/min flow rate and 41 column volumes over 40 min. The first and the second flash chromatography fraction of the extract were subjected to preparative HPLC over a Phenomenex Synergi C_{12} preparative column using an isocratic system of 60:40 of CH_3CN−H_2O (0.1% formic acid) over 45 min at a flow rate of 21.24 mL/min to yield *ent*-shiraiachrome A (**1**, 580 mg), hypocrellin (**2**, 23 mg), hypocrellin B (**3**, 1.4 mg), and hypomycin A (**4**, 4.6 mg). The third flash chromatography fraction was subjected to prep-HPLC using the same protocol to obtain hypomycin C (**5**, 1.3 mg), hypomycin E (**6**, 0.5 mg), and prehypocrellin (**7**, 1.5 mg).

*Prehypocrellin (**7**).* Dark red amorphous powder; UV (CH_3OH) λ_{max} (log ε) 576 (3.74), 470 (4.02), 254 (4.31), 213 (4.46) nm; ^{1}H NMR (700 MHz, $CDCl_3$) and $^{13}C\{^1H\}$ NMR (175 MHz, $CDCl_3$) (see Table S1); HRMS (ESI) m/z: $[M + H]^+$ calcd for $C_{30}H_{27}O_{10}$ 547.1604; Found 547.1583.

Cyclic Voltammetry Measurements. A three-electrode setup was used for all voltammetry experiments with a 3.0 mm glassy carbon disk working electrode, a carbon rod counter electrode, and a leak-free Ag/AgCl reference electrode (3.4 M KCl) inside an OMNI-Lab inert atmosphere (<0.5 ppm of O_2 and H_2O) glovebox filled with nitrogen. The potentials were referenced to the Ag/AgCl electrode. All electrodes were cleaned with acetone and nanopure water before and after use. Acetonitrile was further deoxygenated by bubbling with argon for 45−60 min followed by storage over 3 Å molecular sieves for at least 72 h prior to use. The electrolyte *tetra-n*-butylammonium hexafluorophosphate (98%), $[(n\text{Bu})_4\text{N}][PF_6]$, was purchased from Oakwood Chemicals and further purified by recrystallization from ethanol. OmniPur sodium acetate, trihydrate, and acetic acid (glacial; 100%) were purchased from Millipore Sigma.

Spectroelectrochemistry. A three-electrode setup was used for spectroelectrochemistry experiments with a platinum mesh working electrode, a platinum wire counter electrode, and a leak-free Ag/AgCl reference electrode (3.4 M KCl). The solutions were made inside the glovebox and transferred into a custom-made 1 mm Schlenk cuvette designed specifically for air-free spectroelectrochemistry experiments. The cuvette was then sealed and brought outside of the glovebox to the UV−vis instrument. First, a blank was recorded which consisted of 100 mM of the supporting electrolyte, $[(n\text{Bu})_4\text{N}][PF_6]$, in solution without the electrodes present. Then, a solution containing both electrolyte (100 mM) and compound **1** (248 μM) was added to the cuvette and the UV−vis spectrum was recorded. The electrodes were then inserted into the solution and connected to the potentiostat, and another spectrum was recorded, demonstrating a slight increase in the baseline due to the blockage of the working electrode. This solution was then used for a blank, and subsequent UV−vis difference measurements were recorded as a negative potential was applied to the working electrode. The starting potential was −0.3 V and was decreased by 0.05 V when the UV−vis spectra were unchanging. The final potential applied was −0.850 V.

Small-Scale Reduction of Hypocrellins (1−3) and Hypomycins (4−6) with Sodium Dithionite. Chemical reductions of compounds **1**−**6** using $Na_2S_2O_4$ as a reducing agent were first conducted at a pilot scale, where 1 mg of *ent*-shiraiachrome A (**1**), hypocrellin (**2**), and hypocrellin B (**3**) was placed in a scintillation vial and dissolved separately in 1 mL of acetonitrile. Each solution was then treated with excess $Na_2S_2O_4$ by adding 0.6 mL of aqueous $Na_2S_2O_4$ solution (480 mM) and mixing thoroughly. Similar procedures were followed for the chemical reductions of hypomycin A (**4**), C (**5**), and E (**6**), but using 0.5 mg of each compound. The six reaction vials were left open at room conditions overnight to provide a regular supply of dioxygen. After 24 h, UPLC-HRESIMS data were collected for the reaction mixtures of **1**−**6** as well as for the starting materials, i.e., pure samples of **1**−**6** dissolved in acetonitrile.

Scaled-up Reduction of *ent*-Shiraiachrome A (1) under Aerobic Condition. The scaled up aerobic reduction of *ent*-shiraiachrome A (**1**) was conducted in four replicates. For each reaction, 10 mg of **1** were dissolved in 2.5 mL of CH_3CN and then treated with 3 mL of $Na_2S_2O_4$ solution (960 mM). The reaction mixtures were stirred for 3 h and then left open overnight. After 24 h, the four reaction mixtures were dried and subjected to UPLC-HRESIMS analysis as described above. To purify the resulting products, the four reactions were combined and subjected to a preparative reversed-phase HPLC separation using a Phenomenex Synergi C_{12} preparative column and a gradient system of 50:50 to 60:40 CH_3CN−H_2O (0.1% formic acid) over 15 min at a flow rate of 21 mL/min to obtain compounds **1** (23.6 mg), **8** (1.8 mg), **9** (2.5 mg), and **10** (0.6 mg).

*11-O-Demethyl-ent-shiraiachrome A (**8**).* Dark red amorphous powder; ^{1}H NMR (400 MHz, $CDCl_3$) and $^{13}C\{^1H\}$ NMR (100 MHz, $CDCl_3$) (see Table S4); HRMS (ESI) m/z: $[M + H]^+$ calcd for $C_{29}H_{25}O_{10}$ 533.1447; Found 533.1424. ECD (MeOH) nm ($\Delta\varepsilon$): 270 (+4.5), 350 (−6.0), 445 (+12.4), 563 (−4.0).

*2-O-Demethyl-ent-shiraiachrome A (**9**).* Dark red amorphous powder; ^{1}H NMR (500 MHz, $CDCl_3$) and $^{13}C\{^1H\}$ NMR (125 MHz, $CDCl_3$) (see Table S4); HRMS (ESI) m/z: $[M + H]^+$ calcd for $C_{29}H_{25}O_{10}$ 533.1447; Found 533.1421. ECD (MeOH) nm ($\Delta\varepsilon$): 280 (+5.5), 340 (−1.6), 410 (+5.3), 463 (+4.0), 573 (−0.3).

*2,11-O-Demethyl-ent-shiraiachrome A (**10**).* Dark red amorphous powder; ^{1}H NMR (700 MHz, $CDCl_3$) and $^{13}C\{^1H\}$ NMR (175 MHz, $CDCl_3$) (see Table S4); HRMS (ESI) m/z: $[M + H]^+$ calcd for $C_{28}H_{23}O_{10}$ 519.1291; Found 519.1298. ECD (MeOH) nm ($\Delta\varepsilon$): 238 (−5.6), 300 (+1.73), 348 (−5.0), 438 (+4.1), 558 (−1.3).

Reduction of *ent*-Shiraiachrome A (1) and Hypocrellin (2) under Anaerobic Condition. Anaerobic reduction of **1** was performed in triplicate, where 10 mg of **1** were used in each reaction (total of 30 mg). Under a dry oxygen-free argon atmosphere using a standard Schlenk technique, each sample of **1** was dissolved in 2.5 mL of CH_3CN and then treated with 3 mL of aqueous $Na_2S_2O_4$ solution (960 mM). The reactions were stirred under oxygen-free conditions

https://doi.org/10.1021/acs.joc.1c02639
J. Org. Chem. 2022, 87, 2697−2710

for 30 min before drying *in vacuo*. After 24 h, samples for NMR analysis were prepared in an oxygen-free glovebox. Afterward, UPLC-HRESIMS data were collected for each reaction. Reference standards of **1**−**6** were also analyzed by UPLC-HRESIMS to identify the reaction products by matching their molecular ion peaks and retention times. For the purpose of purifying the observed products (i.e., compounds **2**−**6** and **11**−**12** in Scheme 3), the anaerobic reduction reaction of **1** was scaled up by reacting 50 mg of **1** following the same procedures. The reaction mixture was then subjected to a preparative reversed-phase HPLC separation using a Phenomenex Synergi C_{12} column and an isocratic system of 60:40 CH_3CN−H_2O (0.1% formic acid) for 30 min at a flow rate of 21 mL/min to obtain compounds **1** (31.8 mg), **2** (2.1 mg), **3** (0.2 mg), **5** (2.3 mg), **6** (5.3 mg), **11** (1.6 mg), and **12** (0.5 mg). The anaerobic reduction of hypocrellin (**2**, 4.6 mg) was conducted following a nearly identical protocol to obtain compounds **2** (0.5 mg) and **4** (2.97 mg).

2-Demethoxy-ent-shiraiachrome A (11). Dark red amorphous powder; ^{1}H NMR (400 MHz, $CDCl_3$) and $^{13}C\{^1H\}$ NMR (100 MHz, $CDCl_3$) (see Table S7); HRMS (ESI) m/z: $[M + H]^+$ calcd for $C_{29}H_{25}O_9$ 517.1498; Found 517.1478. ECD (MeOH) nm ($\Delta\varepsilon$): 238 (+4.9), 270 (+6.0), 353 (−6.0), 450 (+11.9), 573 (−2.2).

11-Demethoxy-ent-shiraiachrome A (12). Dark red amorphous powder; ^{1}H NMR (700 MHz, $CDCl_3$) and $^{13}C\{^1H\}$ NMR (175 MHz, $CDCl_3$) (see Table S7); HRMS (ESI) m/z: $[M + H]^+$ calcd for $C_{29}H_{25}O_9$ 517.1498; Found 517.1472.

Encapsulated Nanodroplet Crystallization (ENaCt) of Hypocrellin B (3). The crystallization of hypocrellin B (**3**) was examined via the published ENaCt approach.[38] Stock solutions of hypocrellin B (**3**) were prepared in MeOH, aliquoted into screw top glass vials and allowed to evaporate. Samples of hypocrellin B (**3**) were then dissolved in a range of solvents. Droplets of hypocrellin B (**3**) containing solutions (50 nL) were dispensed via an STP Labtech Mosquito liquid handling robot into 96 well glass plates (SWISSCI LCP Modular, 100 μm spacer) containing either an appropriate crystallization oil (200 nL) or no oil. Plates were sealed with a glass coverslip and allowed to stand at room temperature in the dark. After 14 days plates were assessed visually and by cross-polarized light microscopy for crystal growth. From 288 individual ENaCt experiments, 10 wells (3.4%) contained single crystals suitable for X-ray diffraction analysis. A single crystal grown from 50 nL of a DMSO solution of hypocrellin B (**3**) (~76 mg/mL) (Plate 1, B7) was subjected to single crystal X-ray diffraction analysis (Figure S33).

Wells were opened, with use of a tungsten carbide scriber to remove a small portion of the glass cover slide, and the crystal manipulated using Mitegen Kapton microtools. Crystals were transferred to a glass slide and extracted under oil (Fomblin YR-1800) with a standard Mitegen Kapton loop, and mounted onto an in-house diffractometer [Bruker D8 Vantage, Photon 2, dual Incoatec IμS (Ag/Cu), equipped with an Oxford Cryosystems Cryostream open-flow cooling device and maintained at 150 K] for analysis.

Hypocrellin B (**3**) crystallizes in space group $Pna2_1$ with $Z' = 1$. The crystal contains solvent of crystallization as a DMSO solvate. The main moiety contains intramolecular hydrogen bonds and is weakly bond to neighboring molecules through C−H···O interactions (Figure S34 and Table S5). Crystallographic data of **3** were deposited at the Cambridge Crystallographic Data Centre (deposition numbers: CCDC 2085796).

Encapsulated Nanodroplet Crystallization (ENaCt) of *ent*-Shiraiachrome A (1). The crystallization of *ent*-Shiraiachrome A (**1**) was examined via the published ENaCt approach.[38] Stock solutions of *ent*-shiraiachrome A (**1**) were prepared in DCM, aliquoted into screw top glass vials, and allowed to evaporate. Samples of *ent*-shiraiachrome A (**1**) were then dissolved in a range of solvents. Droplets of *ent*-shiraiachrome A (**1**) containing solutions (50 nL) were dispensed via an STP Labtech Mosquito liquid handling robot into 96 well glass plates (SWISSCI LCP Modular, 100 μm spacer) containing an appropriate crystallization oil (200 nL) or no oil. Plates were sealed with a glass coverslip and allowed to stand at room temperature in the dark. After 14 days, plates were assessed visually and by cross-polarized light microscopy for crystal growth. From 288 individual ENaCt experiments, 96 wells (33%) showed evidence of microcrystalline material (Figure S38), while 1 well (0.3%; Plate 1, A9:50 nL of a DMF solution of *ent*-shiraiachrome A (**1**) (~76 mg/mL) in 200 nL of Fomblin Y) contained single crystals suitable for X-ray diffraction analysis (Figures S39 and S40). Wells were opened, and crystals were analyzed using techniques and instruments identical to the procedure described above for **3**.

ent-Shiraiachrome A (**1**) crystallizes in the $P2_1$ space group, including both dimethylformamide and water molecules from the crystallization. The solvent is heavily disordered and has been omitted from the refined structure using the solvent masking routing in Olex2 with the standard settings. The electron count for the omitted molecules matches well with the calculated contribution to the scattering factors (Figure S40 and Table S6). Crystallographic data of **1** were deposited at the Cambridge Crystallographic Data Centre (deposition numbers: CCDC 2085795).

Computational Methods. Molecular Merck force field (MMFF) and density functional theory (TD-DFT/DFT) calculations were carried out with Spartan'10 (Wave function Inc., Irvine, CA, USA) and GaussView 06 software, respectively. The conformers were optimized using DFT calculations at the B3LYP/cc-pVTZ level in CH_3OH for ECD prediction of **5**. The ECD spectra were generated using SpecDis 1.71 software.[41]

■ ASSOCIATED CONTENT

Supporting Information

The Supporting Information is available free of charge at https://pubs.acs.org/doi/10.1021/acs.joc.1c02639.

Experimental section, high-resolution mass spectrometry (HRESIMS) data of **1**−**13**, UV−vis and ECD spectra of **1**−**11**, 1D and 2D NMR data of **7**−**12**, half-wave potentials ($E_{1/2}$), peak-to-peak separations ($\Delta E_{1/2}$), and anodic/cathodic peak current ratios (i_{pa}/i_{pc}) of **1**−**6**, UPLC-HRESIMS chromatogram of **1**−**6** before and after treatment with as a reducing agent, intramolecular hydrogen-bonding analysis of **1**, **2**, and **4**−**6**, X-ray crystallography of *ent*-shiraiachrome A (**1**) and hypocrellin B (**3**), and ECD calculation of hypomycin C (**5**) (PDF)

Accession Codes

CCDC 2085795−2085796 contain the supplementary crystallographic data for this paper. These data can be obtained free of charge via www.ccdc.cam.ac.uk/data_request/cif, or by emailing data_request@ccdc.cam.ac.uk, or by contacting The Cambridge Crystallographic Data Centre, 12 Union Road, Cambridge CB2 1EZ, UK; fax: +44 1223 336033.

■ AUTHOR INFORMATION

Corresponding Authors

Nicholas H. Oberlies − *Department of Chemistry and Biochemistry, University of North Carolina at Greensboro, Greensboro, North Carolina 27402, United States;* orcid.org/0000-0002-0354-8464; Email: nicholas_oberlies@uncg.edu

Shabnam Hematian − *Department of Chemistry and Biochemistry, University of North Carolina at Greensboro, Greensboro, North Carolina 27402, United States;* orcid.org/0000-0002-0788-7615; Email: s_hemati@uncg.edu

Authors

Zeinab Y. Al Subeh − *Department of Chemistry and Biochemistry, University of North Carolina at Greensboro, Greensboro, North Carolina 27402, United States;* orcid.org/0000-0001-9051-4969

Amy L. Waldbusser − *Department of Chemistry and Biochemistry, University of North Carolina at Greensboro, Greensboro, North Carolina 27402, United States;* orcid.org/0000-0002-1972-5621

Huzefa A. Raja − *Department of Chemistry and Biochemistry, University of North Carolina at Greensboro, Greensboro, North Carolina 27402, United States;* orcid.org/0000-0002-0824-9463

Cedric J. Pearce − *Mycosynthetix, Inc., Hillsborough, North Carolina 27278, United States*

Kin Lok Ho − *Chemistry, School of Natural and Environmental Sciences, Newcastle University, Newcastle upon Tyne NE1 7RU, United Kingdom*

Michael J. Hall − *Chemistry, School of Natural and Environmental Sciences, Newcastle University, Newcastle upon Tyne NE1 7RU, United Kingdom;* orcid.org/0000-0001-6475-9161

Michael R. Probert − *Chemistry, School of Natural and Environmental Sciences, Newcastle University, Newcastle upon Tyne NE1 7RU, United Kingdom*

Complete contact information is available at: https://pubs.acs.org/10.1021/acs.joc.1c02639

Notes

The authors declare the following competing financial interest(s): Nicholas Oberlies is on the Scientific Advisory Board of Mycosynthetix, Inc.

■ ACKNOWLEDGMENTS

This research was supported in part by the National Institutes of Health (US)/National Cancer Institute via Grant P01 CA125066 and by the Medical Research Council (UK) via Grant MR/T000740/1. X-ray crystallography facilities at NCL were supported by the Engineering and Physical Sciences Research Council (UK) via Grant EP/F03637X/1. S.H. and A.L.W. are thankful to the University of North Carolina at Greensboro for the financial support provided in the form of startup funds and the New Faculty Research Award.

■ REFERENCES

(1) Jiang, Y.; Leung, A. W.; Wang, X.; Zhang, H.; Xu, C. Effect of photodynamic therapy with hypocrellin B on apoptosis, adhesion, and migration of cancer cells. *Int. J. Radiat. Biol.* **2014**, *90*, 575.

(2) Qi, S.; Guo, L.; Yan, S.; Lee, R. J.; Yu, S.; Chen, S. Hypocrellin A-based photodynamic action induces apoptosis in A549 cells through ROS-mediated mitochondrial signaling pathway. *Acta Pharm. Sin. B* **2019**, *9*, 279.

(3) Yang, Y.; Wang, C.; Zhuge, Y.; Zhang, J.; Xu, K.; Zhang, Q.; Zhang, H.; Chen, H.; Chu, M.; Jia, C. Photodynamic antifungal activity of hypocrellin A against *Candida albicans*. *Front. Microbiol.* **2019**, *10*, 1810.

(4) Su, Y.; Sun, J.; Rao, S.; Cai, Y.; Yang, Y. Photodynamic antimicrobial activity of hypocrellin A. *J. Photochem. Photobiol. B, Biol.* **2011**, *103*, 29.

(5) Mazzini, S.; Merlini, L.; Mondelli, R.; Scaglioni, L. Conformation and tautomerism of hypocrellins. Revised structure of shiraiachrome A. *J. Chem. Soc., Perkin Trans.* **2001**, *2*, 409.

(6) Al Subeh, Z. Y.; Raja, H. A.; Monro, S.; Flores-Bocanegra, L.; El-Elimat, T.; Pearce, C. J.; McFarland, S. A.; Oberlies, N. H. Enhanced production and anticancer roperties of photoactivated perylenequinones. *J. Nat. Prod.* **2020**, *83*, 2490.

(7) Al Subeh, Z. Y.; Raja, H. A.; Monro, S.; Flores-Bocanegra, L.; El-Elimat, T.; Pearce, C. J.; McFarland, S. A.; Oberlies, N. H. Correction to enhanced production and anticancer properties of photoactivated perylenequinones. *J. Nat. Prod.* **2020**, *83*, 3765.

(8) Liu, W. Z.; Shen, Y. X.; Liu, X. F.; Chen, Y. T.; Xie, J. L. A new perylenequinone from Hypomyces sp. *Chin. Chem. Lett.* **2001**, *12*, 431.

(9) Shen, Y. X.; Liu, W. Z.; Rong, X. G.; Sun, Y. H. Studies on the chemical constituents of a fungus producing perylenequinones. *Acta Pharm. Sin.* **2003**, *38*, 834.

(10) Newman, A. G.; Townsend, C. A. Molecular characterization of the cercosporin biosynthetic pathway in the fungal plant pathogen *Cercospora nicotianae*. *J. Am. Chem. Soc.* **2016**, *138*, 4219.

(11) Chen, H. Q.; Lee, M. H.; Chung, K. R. Functional characterization of three genes encoding putative oxidoreductases required for cercosporin toxin biosynthesis in the fungus *Cercospora nicotianae*. *Microbiology* **2007**, *153*, 2781.

(12) Deng, H.; Gao, R.; Liao, X.; Cai, Y. Genome editing in *Shiraia bambusicola* using CRISPR-Cas9 system. *J. Biotechnol.* **2017**, *259*, 228.

(13) Chooi, Y. H.; Zhang, G.; Hu, J.; Muria-Gonzalez, M. J.; Tran, P. N.; Pettitt, A.; Maier, A. G.; Barrow, R. A.; Solomon, P. S. Functional genomics-guided discovery of a light-activated phytotoxin in the wheat pathogen *Parastagonospora nodorum* via pathway activation. *Environ. Microbiol.* **2017**, *19*, 1975.

(14) Leung, A. W.; Ip, M.; Xu, C. S.; Wang, X. N.; Yung, P. T.; Hua, H. Y. Sonodynamic bactericidal efficacy of hypocrellin A and B against methicillin-resistant *Staphylococcus aureus*. *Hong Kong Med. J.* **2017**, *23*, 36.

(15) Li, Y.-T.; Yang, C.; Wu, Y.; Lv, J.-J.; Feng, X.; Tian, X.; Zhou, Z.; Pan, X.; Liu, S.; Tian, L.-W. Axial chiral binaphthoquinone and perylenequinones from the stromata of *Hypocrella bambusae* are SARS-CoV-2 entry inhibitors. *J. Nat. Prod.* **2021**, *84*, 436.

(16) Sollod, C. C.; Jenns, A. E.; Daub, M. E. Cell surface redox potential as a mechanism of defense against photosensitizers in fungi. *Appl. Environ. Microbiol.* **1992**, *58*, 444.

(17) Daub, M. E.; Leisman, G. B.; Clark, R. A.; Bowden, E. F. Reductive detoxification as a mechanism of fungal resistance to singlet oxygen-generating photosensitizers. *Proc. Natl. Acad. Sci. U. S. A.* **1992**, *89*, 9588.

(18) Daub, M. E.; Herrero, S.; Chung, K.-R. Photoactivated perylenequinone toxins in fungal pathogenesis of plants. *FEMS Microbiol. Lett.* **2005**, *252*, 197.

(19) Daub, M. E.; Ehrenshaft, M. The photoactivated toxin cercosporin as a tool in fungal photobiology. *Physiol. Plant.* **1993**, *89*, 227.

(20) Daub, M. E.; Li, M.; Bilski, P.; Chignell, C. F. Dihydrocercosporin singlet oxygen production and subcellular localization: a possible defense against cercosporin phototoxicity in *Cercospora*. *Photochem. Photobiol.* **2000**, *71*, 135.

(21) Leisman, G. B.; Daub, M. E. Singlet oxygen yields, optical properties, and phototoxicity of reduced derivatives of the photosensitizer cercosporin. *Photochem. Photobiol.* **1992**, *55*, 373.

(22) Amrine, C. S. M.; Raja, H. A.; Darveaux, B. A.; Pearce, C. J.; Oberlies, N. H. Media studies to enhance the production of verticillins facilitated by in situ chemical analysis. *J. Ind. Microbiol. Biotechnol.* **2018**, *45*, 1053.

(23) Al Subeh, Z. Y.; Raja, H. A.; Obike, J. C.; Pearce, C. J.; Croatt, M. P.; Oberlies, N. H. Media and strain studies for the scaled production of cis-enone resorcylic acid lactones as feedstocks for semisynthesis. *J. Antibiot.* **2021**, *74*, 496.

(24) O'Brien, E. M.; Morgan, B. J.; Mulrooney, C. A.; Carroll, P. J.; Kozlowski, M. C. Perylenequinone natural products: total synthesis of hypocrellin A. *J. Org. Chem.* **2010**, *75*, 57.

(25) Mulrooney, C. A.; Morgan, B. J.; Li, X.; Kozlowski, M. C. Perylenequinone natural products: enantioselective synthesis of the oxidized pentacyclic core. *J. Org. Chem.* **2010**, *75*, 16.

(26) O'Brien, E. M.; Li, J.; Carroll, P. J.; Kozlowski, M. C. Synthesis of the cores of hypocrellin and shiraiachrome: diastereoselective 1,8-diketone aldol cyclization. *J. Org. Chem.* **2010**, *75*, 69.

(27) Hu, J.; Sarrami, F.; Li, H.; Zhang, G.; Stubbs, K. A.; Lacey, E.; Stewart, S. G.; Karton, A.; Piggott, Andrew M.; Chooi, Y.-H.

Heterologous biosynthesis of elsinochrome A sheds light on the formation of the photosensitive perylenequinone system. *Chem. Sci.* **2019**, *10*, 1457.
(28) Kishi, T.; Tahara, S.; Taniguchi, N.; Tsuda, M.; Tanaka, C.; Takahashi, S. New perylenequinones from *Shiraia bambusicola*. *Planta Med.* **1991**, *57*, 376.
(29) Wu, H.; Lao, X.-F.; Wang, Q.-W.; Lu, R.-R.; Shen, C.; Zhang, F.; Liu, M.; Jia, L. The shiraiachromes: novel fungal perylenequinone pigments from *Shiraia bambusicola*. *J. Nat. Prod.* **1989**, *52*, 948.
(30) Bogeski, I.; Gulaboski, R.; Kappl, R.; Mirceski, V.; Stefova, M.; Petreska, J.; Hoth, M. Calcium binding and transport by coenzyme Q. *J. Am. Chem. Soc.* **2011**, *133*, 9293.
(31) Zhou, Z.; Takaya, N.; Nakamura, A.; Yamaguchi, M.; Takeo, K.; Shoun, H. Ammonia fermentation, a novel anoxic metabolism of nitrate by fungi. *J. Biol. Chem.* **2002**, *277*, 1892.
(32) Krueger, M. C.; Bergmann, M.; Schlosser, D. Widespread ability of fungi to drive quinone redox cycling for biodegradation. *FEMS Microbiol. Lett.* **2016**, *363*, fnw105.
(33) Pedrini, N.; Ortiz-Urquiza, A.; Huarte-Bonnet, C.; Fan, Y.; Juárez, M. P.; Keyhani, N. O. Tenebrionid secretions and a fungal benzoquinone oxidoreductase form competing components of an arms race between a host and pathogen. *Proc. Natl. Acad. Sci. U. S. A.* **2015**, *112*, No. E3651.
(34) Harms, H.; Schlosser, D.; Wick, L. Y. Untapped potential: exploiting fungi in bioremediation of hazardous chemicals. *Nat. Rev. Microbiol.* **2011**, *9*, 177.
(35) Koch, R. A.; Yoon, G. M.; Aryal, U. K.; Lail, K.; Amirebrahimi, M.; LaButti, K.; Lipzen, A.; Riley, R.; Barry, K.; Henrissat, B.; Grigoriev, I. V.; Herr, J. R.; Aime, M. C. Symbiotic nitrogen fixation in the reproductive structures of a basidiomycete fungus. *Curr. Biol.* **2021**, *31*, 3905.
(36) Wei-Shin, C.; Yuan-Teng, C.; Xiang-Yi, W.; Friedrichs, E.; Puff, H.; Breitmaier, E. Die Struktur des Hypocrellins und seines Photooxidationsproduktes Peroxyhypocrellin. *Liebigs Ann. Chem.* **1981**, *1981*, 1880.
(37) Fang, L. Z.; Qing, C.; Shao, H. J.; Yang, Y. D.; Dong, Z. J.; Wang, F.; Zhao, W.; Yang, W. Q.; Liu, J. K. Hypocrellin D, a cytotoxic fungal pigment from fruiting bodies of the ascomycete *Shiraia bambusicola*. *J. Antibiot.* **2006**, *59*, 351.
(38) Tyler, A. R.; Ragbirsingh, R.; McMonagle, C. J.; Waddell, P. G.; Heaps, S. E.; Steed, J. W.; Thaw, P.; Hall, M. J.; Probert, M. R. Encapsulated nanodroplet crystallization of organic-soluble small molecules. *Chem.* **2020**, *6*, 1755.
(39) Mayhew, S. G. The redox potential of dithionite and SO-2 from equilibrium reactions with flavodoxins, methyl viologen and hydrogen plus hydrogenase. *Eur. J. Biochem.* **1978**, *85*, 535.
(40) Blankenhorn, G.; Moore, E. G. Sulfoxylate ion (HSO_2^-), the hydride donor in dithionite-dependent reduction of NAD+ analogs. *J. Am. Chem. Soc.* **1980**, *102*, 1092.
(41) Bruhn, T.; Schaumloffel, A.; Hemberger, Y.; Bringmann, G. SpecDis: quantifying the comparison of calculated and experimental electronic circular dichroism spectra. *Chirality* **2013**, *25*, 243.

NOTE ADDED AFTER ASAP PUBLICATION

This paper published ASAP on January 25, 2022 with an error in the text. The error was corrected and the revised manuscript reposted on February 15, 2022.

https://doi.org/10.1021/acs.joc.1c02639
J. Org. Chem. 2022, 87, 2697−2710